

Characterization of charge-exchange collisions between ultracold ${}^6\text{Li}$ atoms and ${}^{40}\text{Ca}^+$ ions

R. Saito¹, S. Haze¹, M. Sasakawa¹, R. Nakai¹, M. Raoult², H. Da Silva Jr.², O. Dulieu², and T. Mukaiyama^{1*}

¹*Institute for Laser Science, University of Electro-Communications, Chofugaoka, Chofu, Tokyo 182-8585, Japan*

²*Laboratoire Aimé Cotton, CNRS, Université Paris-Sud, ENS Cachan, Université Paris-Saclay, 91405 Orsay Cedex, France*

(Dated: October 30, 2018)

We investigate the energy dependence and the internal-state dependence of the charge-exchange collision cross sections in a mixture of ${}^6\text{Li}$ atoms and ${}^{40}\text{Ca}^+$ ions in the collision energy range from 0.2 mK to 1 K. Deliberately excited ion micromotion is used to control the collision energy of atoms and ions. The energy dependence of the charge-exchange collision cross section obeys the Langevin model in the temperature range of the current experiment, and the measured magnitude of the cross section is correlated to the internal state of the ${}^{40}\text{Ca}^+$ ions. Revealing the relationship between the charge-exchange collision cross sections and the interaction potentials is an important step toward the realization of the full quantum control of the chemical reactions at an ultralow temperature regime.

I. INTRODUCTION

A system of laser-cooled ions immersed in an ultracold atomic gas introduces a new experimental degree of freedom, a charge, into cold atom experiments [1–15]. A single ultracold ion would be useful as a local probe of an ultracold atomic cloud with high spatial resolution, since ions can be controlled using an electric field without exerting much influence on the atoms [16, 17]. A system of several crystalized ions mixed with neutral atoms would nicely model atomic cores comprising lattice mixed with an electron gas in a solid-state material [18]. The charge of the ions would activate the atoms and ions to chemical reactions, and therefore the atom-ion hybrid system would make an ideal platform to study chemical reactions at a single atom level.

When atoms and ions are trapped together, the ions attract the atoms by their static electric field and sometimes lead to inelastic collisions. So far, charge-exchange collisions either with or without emission of radiation [3, 5–7, 9, 15] and molecular association due to radiative processes [7, 8, 19, 20] or three-body collisions [21–23] have been studied in ultracold atom-ion hybrid systems. A systematic study of such inelastic collisions, which are elementary chemical reaction processes, is essential to realize the full quantum control of the chemical reactions in an ultralow temperature regime. The knowledge of the molecular interaction potentials and the potential couplings is important for understanding such chemical reactions. The experimental characterization of the ultracold inelastic collisions under the precise control of the collision energies and the internal states of the reacting atoms and ions allows for testing the interaction potentials which are obtained from the elaborated quantum chemistry calculations.

In this article, we systematically study the energy

dependence and the internal-state dependence of the charge-exchange cross sections in an ultracold ${}^6\text{Li}$ – ${}^{40}\text{Ca}^+$ mixture. Our choice of the atom-ion combination is unique and promising for the observation of quantum collisions since the ${}^6\text{Li}$ – ${}^{40}\text{Ca}^+$ combination has a high s-wave threshold energy of 10 μK and a quite low limit of micromotion-induced heating rate of a few microkelvin per second [24]. The collision energy in our measurement ranges from 0.2 mK to 1 K, spanning nearly four orders of magnitude. To control the collision energies precisely, we deliberately excite an excess ion micromotion in a linear Paul trap. We determine the energy of the ions from the micromotion-modulated fluorescence spectra [25–27]. The energy dependence of the charge-exchange cross section $\sigma_{\text{CE}}(E)$ is scaled with the energy-dependent Langevin cross section $\sigma_{\text{L}}(E)$ and the cross section can be expressed as $\sigma_{\text{CE}}(E) = A \times \sigma_{\text{L}}(E)$. The factor A describes the probability of undergoing the charge-exchange collision reflecting the details of the potential mixing of the incoming and outgoing channels. We measure A for the ${}^{40}\text{Ca}^+$ ions in the ground $S_{1/2}$ state and the excited $P_{1/2}$, $D_{3/2}$ and $D_{5/2}$ states. We also performed the calculation of the LiCa^+ potential energy curves, and from the comparison between the experimental results with theory calculations, we have identified the route of the charge-exchange collisions. A profound understanding of the interaction potentials is an important step to predict the route for the molecular ion formation, which may allow us to realize the creation of translationally cold molecules composed of large number of atoms, and to reveal the physics of the growth of mesoscopic molecular ions [28].

II. EXPERIMENTAL SETUP

In our experiment, ${}^6\text{Li}$ atoms and ${}^{40}\text{Ca}^+$ ions were trapped and cooled separately in a different part of a vacuum chamber as shown in Fig. 1. After the preparation of the atoms and the ions, the atoms were trans-

* Email address : muka@ils.uec.ac.jp

ferred to the center between the ion trap electrodes using an optical tweezer, and mixed with the ions. The ions were trapped by a conventional linear Paul trap with an RF voltage with amplitude 44 V and frequency $\Omega = 2\pi \times 4.8$ MHz, realizing the radial and the axial trap frequencies of $(\omega_r, \omega_z) = 2\pi \times (252, 95)$ kHz, respectively. Neutral ^{40}Ca atoms from the oven were photoionized using 423 nm and 375 nm lasers. Then the ions were cooled with a 397 nm laser, whose frequency was red-detuned from the $S_{1/2} - P_{1/2}$ transition and with a 866 nm laser, as a repump light, tune to the resonance of the $D_{3/2} - P_{1/2}$ transition. Fluorescence from the ions was detected by a photomultiplier tube (PMT) and an electron multiplying CCD (EMCCD) camera. The ion trap system included compensation electrodes to minimize the excess micromotion of the trapped ions. Minimization of the micromotion was accomplished by the RF photon correlation method, and the residual micromotion energy at the optimum condition was estimated to be $k_B \times 0.2$ mK.

^6Li atoms were first trapped by a conventional magneto-optical trap (MOT) and then transferred into a cavity-enhanced optical dipole trap (ODT) [29]. Eventually, they were transferred into a single optical dipole trap created by a 1064 nm laser [30]. Then, the atoms were transported to the position of the ion trap to create the atom-ion mixture by moving one lens placed on the translation stage. The trap frequencies for the atoms were 670 Hz in the radial direction and 1.7 Hz in the axial direction. The peak density of the atoms was $(4.8 \pm 0.3) \times 10^8 \text{ cm}^{-3}$. The temperature of the ^6Li atoms was $(5.8 \pm 0.1) \mu\text{K}$. ^6Li was prepared in the ground hyperfine state $F = 1/2$ of $^2S_{1/2}$ when they were mixed with the $^{40}\text{Ca}^+$ ions in the current experiment.

III. CALIBRATION OF THE COLLISION ENERGY

We tune the energy of the ions by deliberately exciting the excess micromotion in a controlled way. We start from the condition in which the micromotion of the ions is well compensated, and then we apply an offset electric field to displace the ions in the radial direction (x and y directions) to intentionally add an excess micromotion energy to the ions. The added kinetic energy of the ions is determined from the shape of the ions' fluorescence spectra.

When the micromotion is excited, the spectral shape gets broadened and deformed, as shown in Fig. 2(a). The spectral intensity P can be described as

$$P = \frac{\chi^2}{4} \sum_{n=-\infty}^{\infty} \frac{J_n^2(\beta)}{(\Delta\omega + n\Omega)^2 + (\gamma/2)^2}, \quad (1)$$

where $\Delta\omega$, γ , and χ are the laser detuning, the natural linewidth of the $S_{1/2} - P_{1/2}$ transition, and the electric dipole moment of the transition, respectively, and J_n is the n -th order Bessel function for β [25–27]. The value β

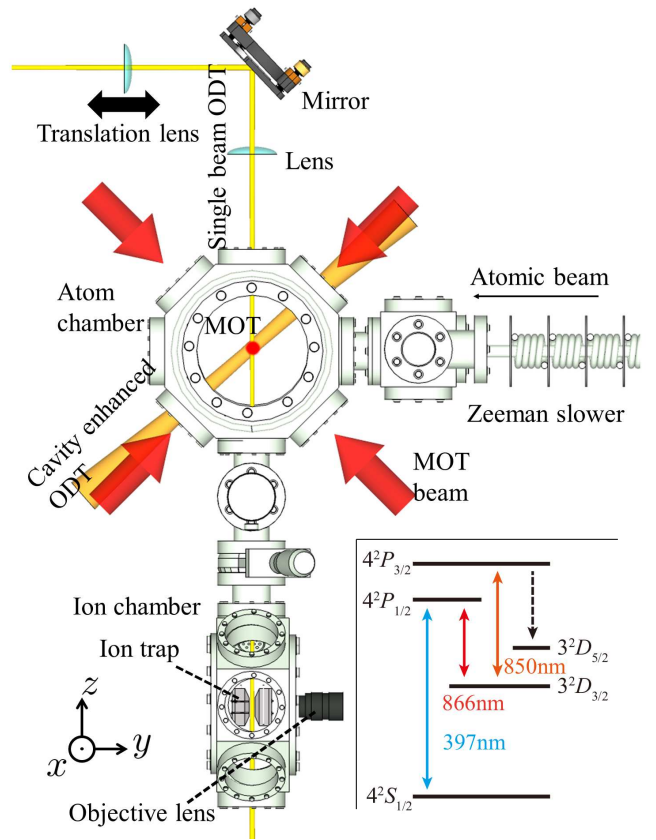


FIG. 1. Schematic drawing of the experimental setup. The upper part shows the atom chamber whereas the lower part presents the ion chamber. ^6Li atoms are supplied from right side of the atom chamber and are decelerated by a Zeeman slower. First, ^6Li atoms are trapped by a conventional MOT, and, then, they are trapped by the cavity-enhanced trap and transferred into an ODT at the center of the atom chamber. Ca^+ ions are trapped at the center of the ion trap electrode placed inside the ion chamber. The 397 nm cooling laser for the ions is incident along both the radial and the axial directions of the ion trap, and the 866 nm repump laser is incident along the axial direction. Fluorescence of the ions is collected by an objective lens and detected by a PMT and EMCCD camera. Energy level diagram of the $^{40}\text{Ca}^+$ ion is shown in the inset.

is the modulation index defined by $\beta = |\frac{k v_r \cos \theta}{\Omega}|$, where k is the wavenumber of the cooling laser, v_r is the velocity of the ion along the direction of the micromotion (namely x and y directions in our case), and θ is the angle of the propagation direction of the cooling laser to the x - y plane, respectively. When $\beta = 0$, the Bessel function can only be $n = 0$, and the spectral shape becomes a simple Lorenz function. When β has a finite value, the spectral shape is deformed and shows a peak around $|\Delta\omega| \approx \beta\Omega$. We determine β by fitting the spectra with Eq. (1).

Figure 2(a) shows the fluorescence intensity of the Ca^+ ions measured by the PMT plotted against cooling laser detuning. The red, green and blue markers indicate the fluorescence spectra obtained at the applied electric field

strength of 0, 3.5, and 10.5 V/m, respectively. The solid red, green and blue curves show the results of the fitting with Eq. (1), and $\beta = 0.24(2), 3.4(1), 7.5(2)$ for the red, green and blue data, respectively.

The excess micromotion energy of the ion E_{emm} is determined by β from the expression [25],

$$E_{\text{emm}} = \frac{m_{\text{ion}}\Omega^2}{2k^2\cos^2\theta}\beta^2, \quad (2)$$

where m_{ion} is the mass of the Ca^+ ion. The total kinetic energy of the Ca^+ ion is

$$E_{\text{ion}} = E_{\text{min}} + E_{\text{emm}}. \quad (3)$$

Here $E_{\text{min}} \approx k_{\text{B}} \times 1.8\text{mK}$ is the minimum energy we can reach in the optimum compensation condition of the micromotions. E_{min} can in principle reach $\frac{3}{2}k_{\text{B}}T_{\text{D}} \approx k_{\text{B}} \times 0.75\text{ mK}$ (T_{D} is the Doppler limit), but the actual value is determined by the quality of the laser cooling.

Figure 2(b) illustrates the kinetic energy of the ion determined from the fluorescence spectra plotted against the applied offset electric field. The electric field is enforced by applying the voltage to the compensation electrode, and the electric field strength is calibrated through the displacement of the ions measured using the CCD camera. The plot shows the quadratic dependence of E_{emm} to the applied electric field which can be described as [31]

$$E_{\text{emm}} = \frac{4}{m_{\text{ion}}} \left(\frac{e\mathcal{E}_r}{q\Omega} \right)^2, \quad (4)$$

where e , \mathcal{E}_r and q are an elementary charge, the applied electric field strength, and the stability parameter of the ion trap, respectively [25, 31, 32]. From the fitting of the data shown in Fig. 2(b) with Eq. (4) by taking q as a free parameter, we obtain $q = 0.12$ from the data (the dashed curve). The dashed curve is used to interpolate the data for the determination of the energy of the ion at the intermediate electric field strength. The collision energy is determined from the ion kinetic energy by $E_{\text{coll}} = (\mu/m_{\text{ion}})E_{\text{ion}}$, where μ is the reduced mass of the ${}^6\text{Li} - {}^{40}\text{Ca}^+$ combination and $\mu/m_{\text{ion}} = 0.13$. Therefore, in ideal conditions, we can in principle reach the collision energy down to factor of eight smaller than the Doppler limit of the Ca^+ ion only by the Doppler cooling.

IV. ENERGY DEPENDENCE OF THE CHARGE-EXCHANGE COLLISION CROSS SECTIONS

The inelastic collisions that we observe in our system have been identified as charge-exchange collisions through the mass spectrometry of the reaction product ions in our previous work [15]. In the current experiment, three to seven Ca^+ ions are loaded in the ion trap to form a one-dimensional crystal. Then ions are mixed

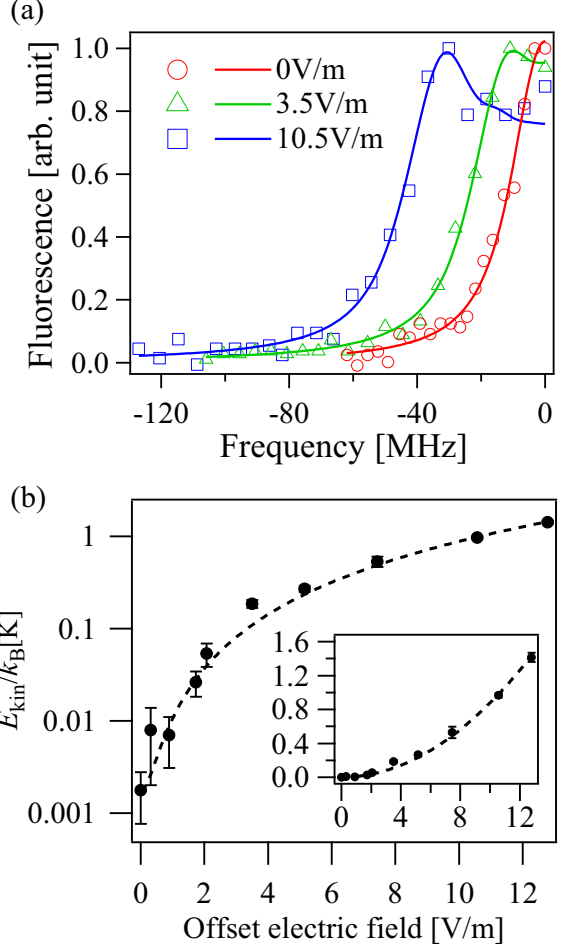


FIG. 2. (a) Fluorescence spectra of the Ca^+ ions for different offset electric fields. Horizontal and vertical axes show the cooling laser detuning and the fluorescence intensity of the ions, respectively. (b) The total kinetic energy of the ion determined from the spectra vs. the offset electric field. Error bars indicate standard errors. The dashed curve shows the result of fitting with the quadratic function to the electric field.

with Li atoms and held for one second, and we count the number of ions lost from the trap. Within one second of the holding, the number of ions decays in time. We repeat the measurement 50 times and the ion-loss probability P_{CE} as a function of holding time is measured. We derive the charge-exchange collision rate Γ_{CE} from the solution of the rate equation which takes into account the radiative decay of the ion from the metastable $D_{3/2}$ and $D_{5/2}$ states, $P_{\text{CE}} = \frac{\Gamma}{\gamma + \Gamma} e^{-(\gamma + \Gamma)t} + \frac{\gamma}{\gamma + \Gamma}$, where γ is the spontaneous decay rate of the $D_{3/2}$ and $D_{5/2}$ states and t is the mixing time of the atoms and ions [15]. The energy-dependent charge-exchange collision cross section $\sigma_{\text{CE}}(E)$ can be derived from the relation $\sigma_{\text{CE}}(E) = \Gamma_{\text{CE}}/nv$, where n is the atomic density and v is the mean relative velocity of the colliding atom and ion. The atomic density n at the ion position is determined from the information on the number of atoms, the

trap frequencies for the atoms, and the displacement of the ion position from the center of the atomic cloud. Although an elastic collision between a Li atom and a Ca^+ ion causes the loss of the atoms, the reduction of the number of atoms in the current experiment is negligible. The relative velocity of the Li atom and the Ca^+ ion is determined solely by the velocity of the ion, since the velocity of the ion is much greater than the velocity of the atom.

Figure 3(a) shows the measured charge-exchange col-

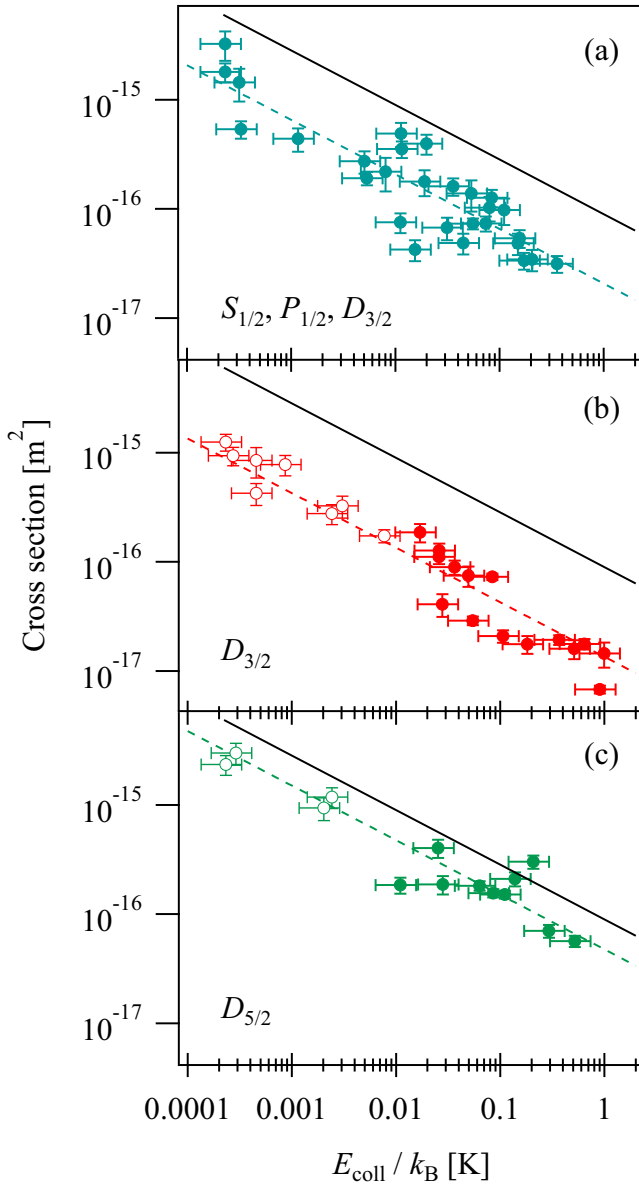


FIG. 3. Charge-exchange collision cross sections as a function of the collision energy for the Ca^+ ions (a) in the superposition of the $S_{1/2}$, $P_{1/2}$ and $D_{3/2}$ states, (b) $D_{3/2}$ state, and (c) $D_{5/2}$ state, respectively. The black solid lines indicate Langevin cross section given by Eq. (5). The dashed lines show the fitting result of the data with the $E^{-1/2}$ dependence predicted from the Langevin model.

lision cross sections as a function of the collision energy E_{coll} for the Ca^+ ions under the irradiation of the cooling and repump lasers. In this condition, ions are considered to be in the superposition state of the $S_{1/2}$, $D_{3/2}$ and $P_{1/2}$ states. The solid line in Fig. 3(a) is the energy-dependent Langevin collision cross section expressed as [33]

$$\sigma_L(E_{\text{coll}}) = \pi \sqrt{\frac{2C_4}{E_{\text{coll}}}} \approx 3.3 \times 10^{-28} \times E_{\text{coll}}^{-1/2} [\text{m}^2], \quad (5)$$

for the ${}^6\text{Li}-{}^{40}\text{Ca}^+$ combination, where $C_4 = \alpha Q^2 / 4\pi\epsilon_0$, α , Q and ϵ_0 are the static polarizability of the ${}^6\text{Li}$ atoms, the charge of the Ca^+ ion and the vacuum permittivity, respectively. Since the charge-exchange collision happens when the atom-ion distance is very small, the charge-exchange collision is a part of the Langevin collision and therefore $\sigma_{\text{CE}}(E_{\text{coll}})$ is proportional to but smaller than $\sigma_L(E_{\text{coll}})$. The energy dependence of the data shown in Fig. 3(a) is consistent with that of the Langevin model in the collision energy range of our measurements.

In order to reveal the internal-state dependence of the charge-exchange collision cross sections, we prepare ${}^{40}\text{Ca}^+$ ions in the various internal states using an optical pumping. To prepare the ion in ground $S_{1/2}$ state, we turn off the cooling laser 20ms earlier than the repump laser. To prepare the ion in the $D_{3/2}$ state, the repump laser is turned off 20ms earlier than the cooling laser. To prepare the ion in the $D_{5/2}$ state, we turn off the repump laser and then the 850 nm laser that drives the ions from $D_{3/2}$ to $P_{3/2}$ is irradiated together with the cooling laser for 20 ms. The pumping of the ions is done just before the atoms are transported to the ion trap position. We have confirmed that the fluctuation of the transportation timing does not affect our measurement of the charge-exchange rate.

Figures 3(b) and (c) show the charge-exchange collision cross sections vs E_{coll} for the Ca^+ ions prepared in the metastable $D_{3/2}$ and $D_{5/2}$ states. In contrast to the case of ions under cooling lasers, ions prepared in the metastable D state is not irradiated by the cooling lasers and therefore ions may be exposed to heating by an RF noise [34, 35]. The rate of the heating arising from the RF noise depends on the spectral density of the electric field noise, which obeys the empirically obtained power law to the ion-electrode distance [34, 35]. We estimate the rate of the heating due to RF noise using the typical value of the spectral density from the power law, and it is estimated to be 70 mK/s for the geometric layout of our ion trap. Since our measurement of the charge-exchange cross section may suffer from the heating due to the RF noise, we exclude the data of the collision energy less than 10 mK (shown with the open markers in Figs. 3(b,c)) from the analysis of energy dependence of the cross sections provided below.

We fit the data shown in Figs. 3(a-c) to the function $\sigma_{\text{CE}}(E_{\text{coll}}) = A \times \sigma_L(E_{\text{coll}})$ with the pre-factor A as a free parameter. The dashed lines in Figs. 3(a-c) are the fitting result to the data. The obtained values of A are

summarized in Table I. To derive A for the $P_{1/2}$ state, we estimate the population distribution of the ion in the $S_{1/2}$, $P_{1/2}$ and $D_{3/2}$ states. From the information on the intensity and the detuning of the cooling and the repump lasers, the population distribution is determined to be $(p_S, p_P, p_D) = (0.42, 0.29, 0.29)$. Since the collision cross section for the mixed state is described as $\sigma_{\text{mixed}} = p_S\sigma_S + p_P\sigma_P + p_D\sigma_D$, a coefficient for the $P_{1/2}$ state is determined from A for the $S_{1/2}$ and $D_{3/2}$ states. As for the ions in the $S_{1/2}$ state, the charge-exchange collision rate is too small to be measured accurately in the current experiment. We have determined the upper limit of A for the $S_{1/2}$ state to be 1×10^{-3} which corresponds to our measurement limit of the smallest charge-exchange rate of 10^{-3} s^{-1} .

V. CALCULATION OF THE POTENTIAL ENERGY CURVES

The knowledge of the molecular properties of the LiCa^+ system yields useful insight to interpret the results above. Surprisingly enough, no information was available in the literature for this system up to now. Following the approach developed in Ref. [36, 37], we calculated the LiCa^+ potential energy curves (PECs) for all symmetries up to the $\text{Li}(2s)+\text{Ca}^+(4p)$ dissociation limit, namely the 9th asymptote. Computing such highly-excited states is indeed easily tractable with our approach. Generally speaking, a diatomic molecules composed of an alkali-metal atom and an alkaline-earth ion can be modeled as a system where the two valence electrons are moving in the field of the two ionic cores Li^+ and Ca^{2+} . The latter are represented by two effective core potentials which include core polarization effects. The Schrödinger equation for the two valence electrons can then be solved in a configuration space spanned by a large Gaussian basis set. With only two active electrons, a full configuration interaction can thus be achieved [36, 37] yielding ground state PEC and numerous excited state PECs, displayed on Fig. 4.

In contrast with heavier systems like RbCa^+ or RbBa^+ [7, 8, 19], the LiCa^+ species is light enough to allow accessing to the PECs up to $\text{Li}(2s)+\text{Ca}^+(4p)$, thus representing an appealing species to sort out the complicated dynamics taking place in such a hybrid trap. Assuming that only two-body reactions are expected in the

TABLE I. A for various internal states of $^{40}\text{Ca}^+$ ions.

$^{40}\text{Ca}^+$ internal state	A
$S_{1/2}$	$\lesssim 1 \times 10^{-3}$
$D_{3/2}$	0.14 ± 0.01
$D_{5/2}$	0.54 ± 0.03
Mixed state of $S_{1/2}$, $P_{1/2}$, and $D_{3/2}$	0.23 ± 0.03
$P_{1/2}$	0.65 ± 0.10

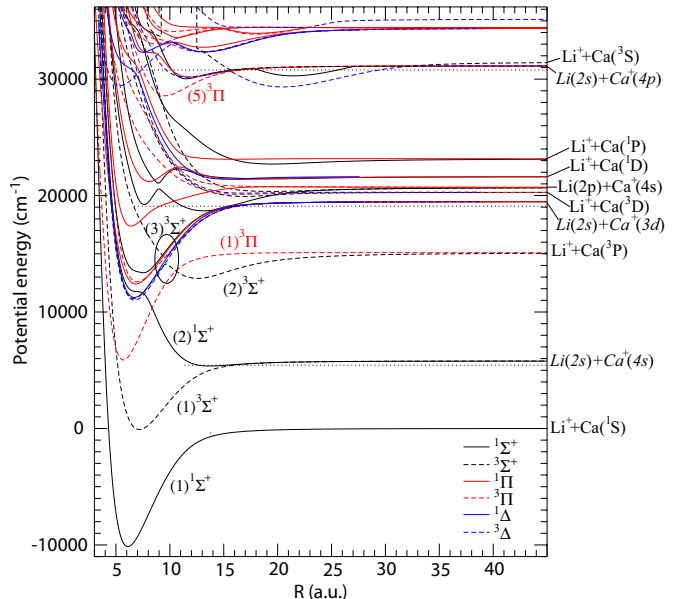


FIG. 4. LiCa^+ potential energy curves computed in the present work relevant for the experiment. The circle locates the avoided crossing which is expected to be active for the charge-exchange process starting from $\text{Li}(2s)+\text{Ca}^+(3d)$ for the $^3\Sigma^+$ symmetry.

present experimental conditions, one can immediately infer several statements allowing to understand the present experimental results. First there is a strong avoided crossing (circled in Fig. 4) between the $(2)^3\Sigma^+$ and the $(3)^3\Sigma^+$ PECs which is probably responsible for the large observed charge exchange rate in the $\text{Li}(2s)+\text{Ca}^+(3d)$ entrance channel. As it is well isolated from other curves, this avoided crossing can be linearized following the standard Landau-Zener approach, so that a single path transition probability can be estimated according to $P_{\text{LZ}} = \exp(-2\pi W_c^2/(v(R_c)\Delta F_c)$. In this expression the interaction strength parameter $W_c = 0.0015025$ a.u. is half of the potential energy spacing between the two PECs at the crossing point located at $R_c = 9.69a_0$ (a_0 is the Bohr radius). The classical relative velocity $v_c = \sqrt{2U_c/\mu} = 0.002082$ a.u. at R_c of the particles with reduced mass μ is obtained through the value $U_c = 0.023533$ a.u. of the potential energy at R_c with respect to the $\text{Li}(2s)+\text{Ca}^+(3d)$, assuming a negligible incoming velocity at large distance. Finally the $\Delta F_c = 0.011612$ a.u. is the difference of slopes between the two branches of the linearized crossing. All together we obtain $P_{\text{LZ}} = 0.556$ which is large enough to explain the large observed charge exchange rate. Note however that several further issues should be taken in account for a more quantitative estimate. First, assuming a statistical population of the initial molecular states, the $(3)^3\Sigma^+$ state would be populated with a weight of $3/20$. On the other hand, spin-orbit interaction probably plays a significant role in the dynamics; in particular, the $(2)^3\Pi$, $(1)^1\Pi$ and $(1)^3\Delta$ state are expected to be efficiently cou-

pled to the $(3)^3\Sigma^+$ state, so that the effective incoming flux toward the avoided crossing is probably higher than the one inferred by the statistical weight. Moreover, the inclusion of the spin-orbit interaction in the model would allow to interpret the observed difference of rates for the $D_{3/2}$ and the $D_{5/2}$ states.

The reported almost unmeasurable rate for the charge exchange reaction starting from the $\text{Li}(2s)+\text{Ca}^+(4s)$ entrance channel is also readily interpreted from the behavior of the PECs. Just like in other similar species [20], two molecular states are correlated to this asymptote, namely the $(1)^3\Sigma^+$ and the $(2)^1\Sigma^+$. The former state is the lowest one in this symmetry so that only elastic collisions are expected in this channel. The latter state lies far above the LiCa^+ electronic ground state so that no clear efficient avoided crossing is present. Therefore the only possible two-body reaction proceeds through spontaneous emission, leading to either radiative charge exchange leading to two ground state species (a Li^+ ion and a neutral Ca atom), or to the formation of a ground state molecular ion LiCa^+ as already reported in Refs. [7]. Following the method exposed in [20], we estimated that the cross section for these radiative processes is about 50 times smaller than the one calculated for RbCa^+ , namely smaller than 10^{-17} cm^2 . It is likely that this process could be observed provided that an improved detection using mass spectrometry is implemented.

Finally, the situation is more involved for the $\text{Li}(2s)+\text{Ca}^+(4p)$ entrance channel. This asymptote is quite well isolated from neighboring ones so that there is no obvious avoided crossing in the relevant PECs. However we see that at almost vanishing initial energy (see the horizontal dotted line in the figure) the $(5)^3\Pi$ PEC crosses several curves correlated to lower asymptotes to which it can be coupled through spin-orbit interaction, thus allowing for efficient charge exchange. An estimate of the transition probability would require a model for the molecular spin-orbit for these states, and thus further quantum chemistry calculations which are out of the scope of the present paper.

VI. CONCLUSION

In conclusion, we have systematically studied the energy dependence and the internal-state dependence of

the charge-exchange collision cross sections for the ${}^6\text{Li}-{}^{40}\text{Ca}^+$ combination. The energy dependence is confirmed to be consistent with the Langevin model in the collision energy range from 0.2 mK to 1 K. Thanks to the relatively large atom-ion mass ratio, we have reached down to 0.2 mK only with the Doppler cooling. This energy is only a factor of 20 higher than the s-wave threshold energy of $10 \mu\text{K}$. It is confirmed that the collision energy in the current work is still in the classical Langevin regime. The inelastic collision rate depends on which internal state the ions are prepared, and the direct comparison between experiment and theory enable us to pin down the route of the charge-exchange process and also to confirm the calculation result of the potential curves with the experiment. Considering that the ${}^6\text{Li}-{}^{40}\text{Ca}^+$ combination has a quite low heating rate arising from a micromotion [24], the ${}^6\text{Li}-{}^{40}\text{Ca}^+$ combination is one of the most promising candidates to investigate the quantum collisions in an atom-ion hybrid system. The detailed understanding of the inelastic collisions and interaction potentials will be an important step toward the realization of the full quantum control of the elementaly processes of chemical reactions in an ultracold temperature regime.

VII. ACKNOWLEDGMENTS

This work is partially supported by JSPS KAKENHI (Grant No. 26287090, 24105006, 15J10722 and JP16J00890). HdS Jr, MR and OD acknowledge the support of the Marie-Curie Initial Training Network COMIQ: Cold Molecular Ions at the Quantum limit of the European Commission under the Grant Agreement 607491. Romain Vexiau is gratefully acknowledged for double-checking the LiCa^+ PECs.

[1] W. W. Smith, O. P. Makarov, and J. Lin, *J. Mod. Opt.* **52**, 2253 (2005).
[2] A. T. Grier, M. Cetina, F. Orućević, and V. Vuletić, *Phys. Rev. Lett.* **102**, 223201 (2009).
[3] C. Zipkes, S. Palzer, L. Ratschbacher, C. Sias, and M. Köhl, *Phys. Rev. Lett.* **105**, 133201 (2010).
[4] C. Zipkes, S. Palzer, C. Sias, and M. Köhl, *Nature* **464**, 388 (2010).
[5] S. Schmid, A. Härtter, and J. H. Denschlag, *Phys. Rev. Lett.* **105**, 133202 (2010).
[6] W. G. Rellergert, S. T. Sullivan, S. Kotochigova, A. Petrov, K. Chen, S. J. Schowalter, and E. R. Hudson, *Phys. Rev. Lett.* **107**, 243201 (2011).
[7] F. H. J. Hall, M. Aymar, N. Bouloufa-Maafa, O. Dulieu, and S. Willitsch, *Phys. Rev. Lett.* **107**, 243202 (2011).
[8] F. H. J. Hall, M. Aymar, M. Raoult, O. Dulieu, and S. Willitsch, *Mol. Phys.* **111**, 1683 (2013).

[9] S. T. Sullivan, W. G. Rellergert, S. Kotochigova, and E. R. Hudson, Phys. Rev. Lett. **109**, 223002 (2012).

[10] L. Ratschbacher, C. Zipkes, C. Sias, and M. Köhl, Nat. Phys. **8**, 649 (2012).

[11] K. Ravi, S. Lee, A. Sharma, G. Werth, and S. A. Rangwala, Nat. Comm. **3**, 1126 (2012).

[12] S. Haze, S. Hata, M. Fujinaga, and T. Mukaiyama, Phys. Rev. A **87**, 052715 (2013).

[13] S. Lee, K. Ravi, and S. A. Rangwala, Phys. Rev. A **87**, 052701 (2013).

[14] L. Ratschbacher, C. Sias, L. Carcagni, J. M. Silver, C. Zipkes, and M. Köhl, Phys. Rev. Lett. **110**, 160402 (2013).

[15] S. Haze, R. Saito, M. Fujinaga, and T. Mukaiyama, Phys. Rev. A **91**, 032709 (2015).

[16] Y. Sherkunov, B. Muzykantskii, N. dAmbrumenil, and B. D. Simons, Phys. Rev. A **79**, 023604 (2009).

[17] C. Kollath, M. Köhl, and T. Giamarchi, Phys. Rev. A **76**, 063602 (2007).

[18] U. Bissbort, D. Cocks, A. Negretti, Z. Idziaszek, T. Calarco, F. Schmidt-Kaler, W. Hofstetter, and R. Gerritsma, Phys. Rev. Lett. **111**, 080501 (2013).

[19] F. H. J. Hall, P. Eberle, G. Hegi, M. Raoult, M. Aymar, O. Dulieu, and S. Willitsch, Mol. Phys. **111**, 2020 (2013).

[20] H. Da Silva Jr, M. Raoult, M. Aymar, and O. Dulieu, New J. Phys. **17**, 045015 (2015).

[21] A. Härter, A. Krükow, A. Brunner, W. Schnitzler, S. Schmid, and J. H. Denschlag, Phys. Rev. Lett. **109**, 123201 (2012).

[22] A. Krükow, A. Mohammadi, A. Härter, J. H. Denschlag, J. Pérez-Ríos, and C. H. Greene, Phys. Rev. Lett. **116**, 193201 (2016).

[23] A. Krükow, A. Mohammadi, A. Härter, and J. H. Denschlag, arXiv:1602.01381

[24] M. Cetina, A. T. Grier, and V. Vuletić, Phys. Rev. Lett. **109**, 253201 (2012).

[25] D. J. Berkeland, J. D. Miller, J. C. Bergquist, W. M. Itano, and D. J. Wineland, J. Appl. Phys. **83**, 5025 (1998).

[26] R. G. DeVoe, J. Hoffnagle, and R. G. Brewer, Phys. Rev. A **39**, 4362 (1989).

[27] R. Blümel, C. Kappler, W. Quint, and H. Walther, Phys. Rev. A **40**, 808 (1989).

[28] R. Côté, V. Kharchenko, and M. D. Lukin, Phys. Rev. Lett. **89**, 093001 (2002).

[29] A. Mosk, S. Jochim, H. Moritz, Th. Elsässer, M. Weidmüller, and R. Grimm, Opt. Lett. **26**, 1837 (2001).

[30] Y. Inada, M. Horikoshi, S. Nakajima, M. Kuwata-Gonokami, M. Ueda, and T. Mukaiyama, Phys. Rev. Lett. **101**, 180406 (2008).

[31] A. Härter, A. Krükow, A. Brunner, and J. Hecker Denschlag, Appl. Phys. Lett. **102**, 221115 (2013).

[32] Z. Meir, T. Sikorsky, R. Ben-shlomi, N. Akerman, Y. Dallal, and R. Ozeri, arXiv:1603.01810.

[33] M. P. Langevin, Ann. Chem. Phys. **5**, 245 (1905).

[34] M. Brownnutt, M. Kumph, P. Rabl, and R. Blatt, Rev. Mod. Phys. **87**, 1419 (2015).

[35] D. J. Wineland and C. Monroe and W. M. Itano and D. Leibfried and B. E. King and D. M. Meekhof, J. Res. Natl. Inst. Stand. Technol. **103**, 259 (1998).

[36] M. Aymar and R. Guérout and O. Dulieu, J. Chem. Phys. **135**, 064305 (2011).

[37] M. Aymar and O. Dulieu, J. Phys. B **45**, 215103 (2012).